RESEARCH ARTICLE

Parametrizing the Energy Dissipation Rate in Stably Stratified Flows

Sukanta Basu[1] · **Ping He[2]** · **Adam W. DeMarco[3]**

Abstract
We use a database of direct numerical simulations to evaluate parametrizations for energy dissipation rate in stably stratified flows. We show that shear-based formulations are more appropriate for stable boundary layers than commonly used buoyancy-based formulations. As part of the derivations, we explore several length scales of turbulence and investigate their dependence on local stability.

Keywords Buoyancy length scale · Integral length scale · Outer length scale · Ozmidov scale · Stable boundary layer

1 Introduction

Energy dissipation rate is a key variable for characterizing turbulence (Vassilicos 2015). It is a sink term in the prognostic equation of turbulence kinetic energy (TKE; $\overline{e}$)

$$\frac{\partial \overline{e}}{\partial t} + ADV = BNC + SHR + TRP + PRC - \overline{\varepsilon}, \tag{1}$$

where, $\overline{\varepsilon}$ is the mean energy dissipation rate. The terms ADV, BNC, SHR, TRP, and PRC refer to advection, buoyancy production (or destruction), shear production, transport, and pressure correlation terms, respectively. Energy dissipation rate also appears in the celebrated "$-5/3$ law" of Kolmogorov (1941) and Obukhov (1941a, b)

$$E(\kappa) \approx \overline{\varepsilon}^{2/3} \kappa^{-5/3}, \tag{2}$$

✉ Sukanta Basu
s.basu@tudelft.nl

Ping He
drpinghe@umich.edu

Adam W. DeMarco
awdemarc@ncsu.edu

[1] Faculty of Civil Engineering and Geosciences, Delft University of Technology, Delft, The Netherlands

[2] Department of Aerospace Engineering, University of Michigan, Ann Arbor, USA

[3] United States Air Force, Washington, D.C., USA

where, $E(\kappa)$ and κ denote the energy spectrum and wavenumber, respectively.

In field campaigns or laboratory experiments, direct estimation of $\overline{\varepsilon}$ has always been a challenging task as it involves measurements of nine components of the strain rate tensor. Thus, several approximations (e.g., isotropy, Taylor's hypothesis) have been utilized and a number of indirect measurement techniques (e.g., scintillometers, lidars) have been developed over the years. In parallel, a significant effort has been made to correlate $\overline{\varepsilon}$ with easily measurable meteorological variables. For example, several flux-based and gradient-based similarity hypotheses have been proposed (e.g., Wyngaard and Coté 1971; Wyngaard et al. 1971; Thiermann and Grassl 1992; Hartogensis and de Bruin 2005).

In addition, a handful of papers also attempted to establish relationships between $\overline{\varepsilon}$ and either the vertical velocity variance (σ_w^2) or TKE ($\overline{e}$). One of the first relationships was proposed by Chen (1974). By utilizing the Kolmogorov–Obukhov spectrum (i.e., Eq. 2) with certain assumptions, he derived

$$\overline{\varepsilon} \propto \sigma_w^3, \tag{3}$$

where, the proportionality constant is not dimensionless. Since this derivation is only valid in the inertial range of turbulence, a band-pass filtering of vertical velocity measurements was recommended prior to computing σ_w. A few years later, Weinstock (1981) revisited the work of Chen (1974) and again made use of Eq. 2, albeit with different assumptions (see Appendix 2 for details). He arrived at the following equation

$$\overline{\varepsilon} \approx \sigma_w^2 N, \tag{4}$$

where, N is the so-called Brunt–Väisäla frequency. Using observational data from the stratosphere, Weinstock (1981) demonstrated the superiority of Eq. 4 over Eq. 3. In a recent empirical study, by analyzing measurements from the CASES-99 (the Cooperative Atmosphere–Surface Exchange Study–1999) field campaign, Bocquet et al. (2011) proposed to use $\overline{\varepsilon}$ as a proxy for σ_w^2.

In the present work, we quantify the relationship between $\overline{\varepsilon}$ and $\overline{e}$ (as well as between $\overline{\varepsilon}$ and σ_w) by using turbulence data generated by direct numerical simulation (DNS). To this end, we first compute several well-known "outer" length scales (e.g., buoyancy length scale and Ozmidov scale), normalize them appropriately, and explore their dependence on height-dependent stability. Next, we investigate the inter-relationships of certain (normalized) outer length scales that portray qualitatively similar stability-dependence. By analytically expanding these relationships, we arrive at two $\overline{\varepsilon}$–$\overline{e}$ and two $\overline{\varepsilon}$–σ_w formulations; only the shear-based formulations portray quasi-universal scaling.

The organization of this paper is as follows. In Sect. 2, we describe our DNS runs and subsequent data analyses. Simulated results pertaining to various length scales are included in Sect. 3. The $\overline{\varepsilon}$–$\overline{e}$ and $\overline{\varepsilon}$–σ_w formulations are derived in Sect. 4. We discuss the surface-layer characteristics of a specific shear-based length scale in Sect. 5. A few concluding remarks, including the implications of our results for atmospheric modelling, are made in Sect. 6. In order to enhance the readability of the paper, either a heuristic or an analytical derivation of all the length scales is provided in Appendix 1. Given the importance of Eq. 4, its derivation is also summarized in Appendix 2. In Appendix 3, we elaborate on the normalization of various variables that are essential for the post-processing of DNS-generated data. Finally, supplementary results based on our DNS database are included in Appendix 4.

2 Direct Numerical Simulation

Over the past decade, due to the increasing abundance of high-performance computing resources, several studies probed different types of stratified flows by using DNS (e.g., Flores and Riley 2011; García-Villalba and del Álamo 2011; Brethouwer et al. 2012; Chung and Matheou 2012; Ansorge and Mellado 2014; Shah and Bou-Zeid 2014; He and Basu 2015, 2016a). These studies provided valuable insights into the dynamical and statistical properties of these flows (e.g., intermittency, structure parameters). In the present study, we use a DNS database, which was previously generated by using a massively parallel DNS code, called HERCULES (He 2016), for the parametrization of optical turbulence (He and Basu 2016b). The verification of HERCULES has been presented in the appendix of He (2016). We solved the normalized Navier–Stokes and temperature equations in an open-channel flow driven by a streamwise pressure gradient, as shown below (using Einstein's summation notation for subscripts i and j)

$$\frac{\partial u_{n,i}}{\partial x_{n,i}} = 0, \tag{5}$$

$$\frac{\partial u_{n,i}}{\partial t_n} + \frac{\partial u_{n,i}u_{n,j}}{\partial x_{n,j}} = -\frac{\partial p_n}{\partial x_{n,i}} + \frac{1}{Re_b}\frac{\partial}{\partial x_{n,j}}\left(\frac{\partial u_{n,i}}{\partial x_{n,j}}\right) + \Delta P\delta_{i1} + Ri_b\theta_n\delta_{i3}, \tag{6}$$

$$\frac{\partial \theta_n}{\partial t_n} + \frac{\partial \theta_n u_{n,i}}{\partial x_{n,i}} = \frac{1}{Re_b Pr}\frac{\partial}{\partial x_{n,i}}\left(\frac{\partial \theta_n}{\partial x_{n,i}}\right), \tag{7}$$

where u_n and x_n are the normalized velocity and coordinate vectors, respectively, with the subscript i denoting the ith vector component; t_n is the normalized time; p_n is the normalized pressure; ΔP is the streamwise pressure gradient to drive the flow; and θ_n is the normalized potential temperature. The normalization of DNS variables is shown in Appendix 3. Throughout the paper, the subscript "n" is used to denote a normalized variable.

The computational domain size for all the DNS runs was $L_x \times L_y \times L_z = 18h \times 10h \times h$, where h is the open-channel depth. The domain was discretized by $2304 \times 2048 \times 288$ grid points in streamwise, spanwise, and wall-normal directions, respectively. The bulk Reynolds number, Re_b, for all the simulations was fixed at 20000, defined as

$$Re_b = U_b h/\nu, \tag{8}$$

where, ν and U_b denote kinematic viscosity and the bulk (averaged) velocity in the channel, respectively. The constant Re_b was achieved by dynamically adjusting ΔP in Eq. 6 during the simulations. The corresponding friction Reynolds number (Re_τ) ranges from 575 to 902. The bulk Richardson number was calculated as

$$Ri_b = \frac{\left(\theta_{top} - \theta_{bot}\right) gh}{U_b^2 \theta_{top}}, \tag{9}$$

where θ_{top} and θ_{bot} represent potential temperature at the top and the bottom of the channel, respectively. The acceleration due to gravity is denoted by g.

A total of five simulations were performed with gradual increase in the temperature difference between the top and bottom walls (effectively by increasing Ri_b) to mimic the night-time cooling of the land surface. The normalized cooling rates (CR), $\partial Ri_b/\partial T_n$, ranged from 1×10^{-3} to 5×10^{-3}, where T_n is a non-dimensional time ($= tU_b/h$). All our simulations started with fully developed neutral conditions: $Ri_b = 0$. After $T_n = 100$, each simulation evolved to a different Ri_b value, ranging from 0.1 to 0.5. Since we were considering atmo-

spheric flows, the Prandtl number, $Pr = \nu/k$ was assumed to be equal to 0.7, with k being the thermal diffusivity.

The simulation results were output every 10 non-dimensional timestep. To avoid spin-up issues, we only use data of the last five output files (i.e., $60 \leq T_n \leq 100$). Furthermore, we only consider data from the region $0.1h \leq z \leq 0.5h$ to discard any blocking effect of the surface or avoid any laminarization in the upper part of the open channel.

The TKE and its mean dissipation are computed as follows (using Einstein's summation notation)

$$\overline{e} = \frac{1}{2}\overline{u_i' u_i'}, \tag{10a}$$

$$\overline{\varepsilon} = \nu \overline{\left(\frac{\partial u_i'}{\partial x_j} \frac{\partial u_i'}{\partial x_j} \right)}. \tag{10b}$$

In these equations and in the rest of the paper, the "overbar" notation is used to denote mean quantities. Horizontal (planar) averaging operation is performed for all the cases. The "prime" symbol is used to represent the fluctuation of a variable with respect to its planar averaged value.

3 Length Scales

In this section, we discuss various length scales of turbulence. To enhance the readability of the paper, we do not elaborate on their derivations or physical interpretations here; for such details, the readers are directed to Appendix 1.

From the DNS-generated data, we first calculate the integral length scale ($\mathcal{L}$) and Kolmogorov length scale (η). They are defined as (Tennekes and Lumley 1972; Pope 2000)

$$\mathcal{L} \equiv \frac{\overline{e}^{3/2}}{\overline{\varepsilon}}, \tag{11a}$$

$$\eta \equiv \left(\frac{\nu^3}{\overline{\varepsilon}} \right)^{1/4}. \tag{11b}$$

In Fig. 1, normalized values of $\mathcal{L}$ and η are plotted against the gradient Richardson number ($Ri_g = N^2/S^2$), where S is the magnitude of wind shear. Parameters N and S are computed as follows

$$N = \sqrt{\frac{g}{\Theta_0} \frac{\partial \overline{\theta}}{\partial z}}, \tag{12a}$$

$$S = \sqrt{\left(\frac{\partial \overline{u}}{\partial z} \right)^2 + \left(\frac{\partial \overline{v}}{\partial z} \right)^2}, \tag{12b}$$

where Θ_0 is a reference temperature. As mentioned earlier, the overbar denotes horizontal (planar) averaging operation. In the left panel, we marked four specific points based on the data from DNS run with imposed cooling rate of 10^{-3} to better understand the effects of height and stability on the integral length scale. The points p_1 and p_2 represent data from $z/h = 0.1$ and $z/h = 0.5$, respectively, at non-dimensional time (T_n) of 60. Similarly, q_1 and q_2 are associated with data from $z/h = 0.1$ and $z/h = 0.5$, respectively, at non-dimensional time (T_n) of 100.
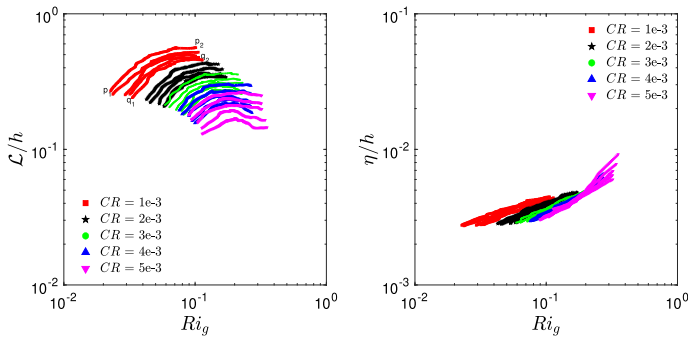
Fig. 1 Integral (left panel) and Kolmogorov (right panel) length scales as functions of gradient Richardson number. Both the length scales are normalized by the height of the open channel (h). Simulated data from five different DNS runs are represented by different coloured symbols in these plots. In the legends, CR represents normalized cooling rates. The points p_1 and p_2 represent data from $z/h = 0.1$ and $z/h = 0.5$, respectively, at non-dimensional time (T_n) of 60. Similarly, q_1 and q_2 are associated with data from $z/h = 0.1$ and $z/h = 0.5$, respectively, at non-dimensional time (T_n) of 100

Physically, one would expect the integral scale to increase with height as long as the eddies feel the presence of the surface (near-neutral or weakly stable condition). For very stable conditions, the eddies no longer feel the presence of the surface. In the atmospheric boundary layer literature, it is known as the *z*-less condition (Wyngaard 1973; Grisogono 2010). Under the influence of strong stability, the integral length scales become more or less independent of the height above the surface.

From Fig. 1, it is clear that the integral length scale increases with height and slowly decreases with time in all the simulations due to the increasing stability effects. Simulations with higher cooling rates have smaller integral length scales. Some of these runs (e.g., $CR = 5 \times 10^{-3}$) exhibit *z*-less behaviour due to strong stability effects.

In contrast, η marginally increases with higher stability due to lower $\bar{\varepsilon}$. The ratio of $\mathcal{L}$ to η decreases from about 100 to 20 as stability is increased from a weakly stable condition to a strongly stable condition.

Next, we compute four outer length scales: Ozmidov (L_{OZ}), Corrsin (L_C), buoyancy (L_b), and Hunt (L_H). They are defined as (Corrsin 1958; Dougherty 1961; Ozmidov 1965; Brost and Wyngaard 1978; Hunt et al. 1988, 1989; Sorbjan and Balsley 2008; Wyngaard 2010)

$$L_{OZ} \equiv \left(\frac{\bar{\varepsilon}}{N^3} \right)^{1/2}, \tag{13a}$$

$$L_C \equiv \left(\frac{\bar{\varepsilon}}{S^3} \right)^{1/2}, \tag{13b}$$

$$L_b \equiv \frac{\bar{e}^{1/2}}{N}, \tag{13c}$$

$$L_H \equiv \frac{\bar{e}^{1/2}}{S}. \tag{13d}$$

Please note that, in the literature, L_b and L_H have also been defined as σ_w/N and σ_w/S, respectively. Both L_{OZ} and L_C are functions of $\bar{\varepsilon}$, a microscale variable. In contrast, L_b and L_H only depend on macroscale variables.
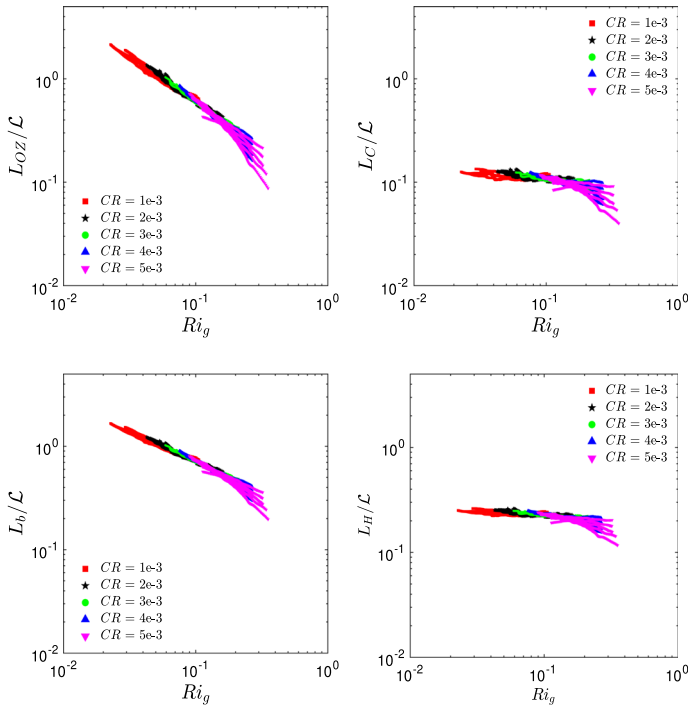
Fig. 2 Ozmidov (top-left panel), Corrsin (top-right panel), buoyancy (bottom-left panel), and Hunt (bottom-right panel) length scales as functions of gradient Richardson numbers. All the length scales are normalized by the integral length scale. Simulated data from five different DNS runs are represented by different coloured symbols in these plots. In the legends, *CR* represents normalized cooling rates

Both shear and buoyancy deform the larger eddies more compared to the smaller ones (Itsweire et al. 1993; Smyth and Moum 2000; Chung and Matheou 2012; Mater et al. 2013). Eddies that are smaller than L_C or L_H are not affected by shear. Similarly, buoyancy does not influence the eddies of size less than L_{OZ} or L_b. In other words, the eddies can be assumed to be isotropic if they are smaller than all these outer length scale.

Since $\mathcal{L}$ changes across the simulations, all the outer length scale are normalized by corresponding $\mathcal{L}$ values and plotted as functions of Ri_g in Fig. 2. The collapse of the data from different runs, on to seemingly universal curves, is remarkable for all the cases except for $Ri_g > 0.2$. We would like to mention that similar scaling behaviour was not found if other normalization factors were used. For instance, we have tried the height of the open channel (h) as a normalization factor. We also tested several definitions of the boundary-layer height (e.g., the height where variances or fluxes decrease to a small percentage of the peak magnitude). None of them resulted in any scaling relationship.

Both normalized L_{OZ} and L_b decrease monotonically with Ri_g; however, the slopes are quite different. The length scales L_C and L_H barely exhibit any sensitivity to Ri_g (except for $Ri_g > 0.1$). Even for weakly stable conditions, these length scales are less than 25 percent of $\mathcal{L}$.
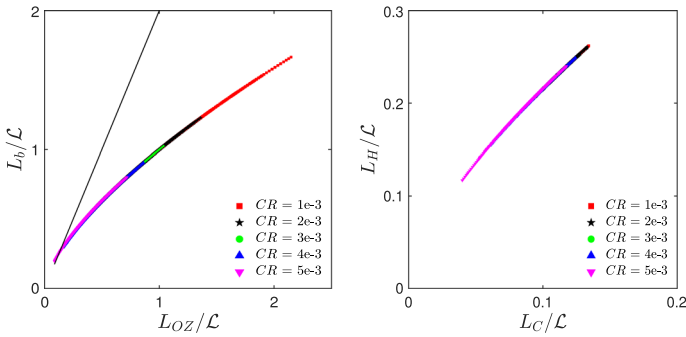
Fig. 3 Left panel: variation of the normalized buoyancy length scale against the normalized Ozmidov length scale. Right panel: variation of the normalized Hunt length scale against the normalized Corrsin length scale. Simulated data from five different DNS runs are represented by different coloured symbols in these plots. In the legends, *CR* represents normalized cooling rates

Based on the expressions of the outer length scale (i.e., Eq. 13a–d) and the definition of the gradient Richardson number, we can write

$$\frac{L_C}{L_{OZ}} = \left(\frac{N}{S}\right)^{3/2} = Ri_g^{3/4}, \tag{14a}$$

$$\frac{L_H}{L_b} = \left(\frac{N}{S}\right) = Ri_g^{1/2}. \tag{14b}$$

Thus, for $Ri_g < 1$, one expects $L_C < L_{OZ}$ and $L_H < L_b$. Such relationships are fully supported by Fig. 2. In comparison to the buoyancy effects, the shear effects are felt at smaller length scales for the entire stability range considered in the present study.

Owing to their similar scaling behaviours, $L_b/\mathcal{L}$ against $L_{OZ}/\mathcal{L}$ are plotted in Fig. 3 (left panel). Once again, all the simulated data collapse nicely in a quasi-universal (nonlinear) curve. Since in a double-logarithmic representation (not shown) this curve is linear, we can write

$$\frac{L_b}{\mathcal{L}} \equiv \left(\frac{L_{OZ}}{\mathcal{L}}\right)^m, \tag{15}$$

where, m is an unknown power-law exponent. Via regression analysis, we estimate $m = 2/3$. By using $L_b \equiv \bar{e}^{1/2}/N$, and the definitions of L_{OZ} and $\mathcal{L}$, we arrive at

$$\frac{\bar{e}^{1/2}}{N} = \left(\frac{\bar{\varepsilon}}{N^3}\right)^{m/2} \left(\frac{\bar{e}^{3/2}}{\bar{\varepsilon}}\right)^{1-m}. \tag{16}$$

Further simplification leads to: $\bar{\varepsilon} = \bar{e}N$; please note that the exponent m cancels out in the process. Instead of $\bar{e}^{1/2}$, if we utilize σ_w in the definitions of L_b and $\mathcal{L}$, we get: $\bar{\varepsilon} = \sigma_w^2 N$. This equation is identical to Eq. 4, which was derived by Weinstock (1981). His derivation, based on inertial-range scaling, is summarized in Appendix 2.

In the right panel of Fig. 3, we plot $L_H/\mathcal{L}$ versus $L_C/\mathcal{L}$. Both these normalized length scales have limited ranges; nonetheless, they are proportional to one another. Like Eq. 15, we can write in this case

$$\frac{L_H}{\mathcal{L}} \equiv \left(\frac{L_C}{\mathcal{L}}\right)^n, \tag{17}$$
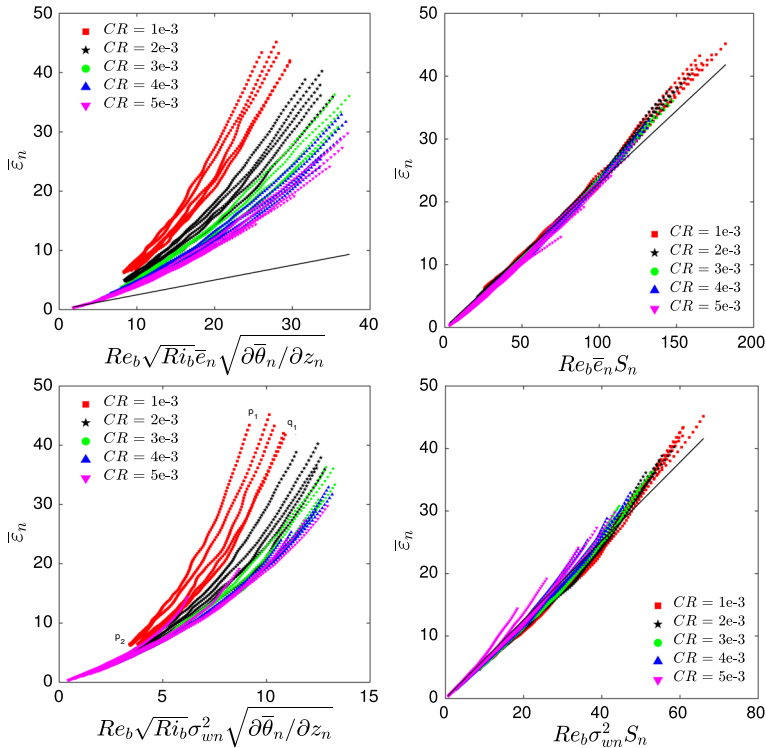
Fig. 4 Variation of normalized energy dissipation rates against normalized $\bar{e}N$ (top-left panel), normalized $\bar{e}S$ (top-right panel), normalized $\sigma_w^2 N$ (bottom-left panel), and normalized $\sigma_w^2 S$ (bottom-right panel). Simulated data from five different DNS runs are represented by different coloured symbols in these plots. In the legends, CR represents normalized cooling rates. In the bottom-left panel, the points p_1 and p_2 represent data from $z/h = 0.1$ and $z/h = 0.5$, respectively at non-dimensional time (T_n) of 60. Whereas, q_1 is associated with data from $z/h = 0.1$ at non-dimensional time (T_n) of 100

where, n estimated via regression analysis is also found to be equal to 2/3. The expansion of this equation leads to either $\bar{\varepsilon} = \bar{e}S$ or $\bar{\varepsilon} = \sigma_w^2 S$, depending on the definition of L_H and $\mathcal{L}$.

4 Parametrizing the Energy Dissipation Rate

Earlier in Fig. 3, we plotted normalized outer length scales against one another. It is plausible that the apparent data collapse is simply due to self-correlation as the same variables (i.e., $\mathcal{L}$, N, and S) appear in both abscissa and ordinate. To further probe into this problematic issue, we produce Fig. 4. Here, we basically plot normalized $\bar{\varepsilon}$ as functions of normalized $\bar{e}N$, $\bar{e}S$, $\sigma_w^2 N$, and $\sigma_w^2 S$, respectively. These plots have completely independent abscissa and ordinate terms and do not suffer from self-correlation. Please note that the appearance of Re_b and Ri_b in these figures is due to the normalization of variables in DNS. The definitions of all the normalized variables (e.g., $\bar{\varepsilon}_n$) are provided in Appendix 3.

It is clear that the plots in the left panel of Fig. 4, which involve N, do not show any universal scaling. For low CR values, normalized $\bar{\varepsilon}$ values do not go to zero; this behaviour is physically realistic. One cannot expect $\bar{\varepsilon}$ to go to zero for neutral condition (i.e., $N \to 0$).

With increasing cooling rates, the curves seem to converge to an asymptotic curve that passes through the origin. As $\bar{e}$ or σ_w continually reduces with increasing stability, one does expect $\bar{\varepsilon}$ to approach zero.

In a seminal paper, Deardorff (1980) proposed a parametrization for $\bar{\varepsilon}$, which for strongly stratified conditions approaches $0.25\bar{e}N$. In Fig. 4 (top-left panel), we overlaid $\bar{\varepsilon} = 0.25\bar{e}N$ on the DNS-generated data. Clearly, it only overlaps with the simulated data in the strongly stratified region. If $\bar{\varepsilon} = 0.25\bar{e}N$ is used in the definition of L_{OZ}, after simplification, one gets $L_{OZ} = L_b/2$. The line $L_b = 2L_{OZ}$ is drawn in Fig. 3. As would be anticipated, it only overlaps with the simulated data when the outer length scales are the smallest (signifying strongly stable condition).

Compared to the left panels, the right panels of Fig. 4 portray very different scaling characteristics. All the data collapse on quasi-universal curves remarkably, especially, for the $\bar{\varepsilon} \approx \bar{e}S$ case. The slopes of the regression lines, estimated via conventional least-squares approach and bootstrapping (Efron 1982; Mooney et al. 1993), are shown on these plots. Essentially, we have found

$$\bar{\varepsilon} = 0.23\bar{e}S, \tag{18a}$$
$$\bar{\varepsilon} = 0.63\sigma_w^2 S. \tag{18b}$$

We note that our estimated coefficient 0.63 is within the range of values reported by Schumann and Gerz (1995) from laboratory experiments and large-eddy simulations (please refer to their Fig. 1).

In summary, neither $\bar{\varepsilon} = \bar{e}N$ nor $\bar{\varepsilon} = \sigma_w^2 N$ are appropriate parametrizations for weakly or moderately stratified conditions; they may provide reasonable predictions for very stable conditions. In contrast, the shear-based parametrizations should be applicable from a wide range of stability conditions, from near-neutral to at least $Ri_g \approx 0.2$. Since within the continuously turbulent stable boundary layer (SBL), Ri_g rarely exceeds 0.2 (see Garratt 1982; Nieuwstadt 1984), we believe Eq. 18a or Eq. 18b will suffice for most practical boundary-layer applications. However, for intermittently turbulent SBLs and the free atmosphere, where Ri_g can exceed O(1), Deardorff's parametrization (i.e., $\bar{\varepsilon} = 0.25\bar{e}N$) might be a more viable option. Unfortunately, we cannot verify this speculation using our existing DNS dataset.

5 Discussions

Hunt et al. (1988, 1989) stated that L_H may not be a representative length scale near the surface due to the blocking effect. From our perspective, L_H does possess the correct surface-layer characteristics, as elaborated below.

Following Nieuwstadt's local scaling (Nieuwstadt 1984) and Monin–Obukhov similarity theory, we can rewrite L_H as follows for the surface layer:

$$L_H \equiv \frac{\bar{e}^{1/2}}{S} \approx \frac{cu_*}{S} = \frac{c\kappa z}{\phi_m}, \tag{19}$$

where, u_* and ϕ_m denote surface friction velocity and non-dimensional velocity gradient, respectively, κ is the von Kármán constant. Based on data from the Cabauw tower in the Netherlands, Nieuwstadt (1984) reported the proportionality constant c to be approximately equal to 2.1. A similar value was also reported by Basu and Porté-Agel (2006).

Since L_H is proportional to κz in the surface layer, it can be directly compared with the so-called master length scale (L_M) of Mellor and Yamada (1982). They proposed

$$\overline{\varepsilon} = \frac{q^3}{B_1 L_M}, \tag{20}$$

where, q equals $(2\overline{e})^{1/2}$ and B_1 is a constant. Various forms of L_M exist in the literature; however, all of them reduce to κz in the surface layer.

If we replace L_M with L_H in Eq. 20, then by utilizing Eq. 18a, we arrive at

$$B_1 = \frac{q^3}{0.23\overline{e}^{3/2}} = 12.3. \tag{21}$$

Based on various observational data, Mellor and Yamada (1982) recommended B_1 to be equal to 16.6. By using data from large-eddy simulations, Nakanishi (2001) recommended $B_1 = 24.0$. Interestingly, Janjić (2002) heuristically derived $B_1 = 11.877992$ (see also Foreman and Emeis 2012). This value of B_1 is currently used in the popular MYJ planetary boundary-layer scheme of the Weather Research and Forecasting (WRF) model. It is quite a coincidence that our DNS-based result turn out to be very close to an earlier proposition by Janjić.

6 Concluding Remarks

The boundary-layer community almost always utilizes buoyancy-based energy dissipation rate parametrizations for numerical modelling studies. Our DNS-based results suggest that shear-based parametrizations are more appropriate for regions of the stable boundary layer where Ri_g does not exceed 0.2. This finding is in complete agreement with the theoretical work (supported by numerical results) of Hunt et al. (1988). They concluded:

> ...when the Richardson number is less than half, it is the mean shear ... (rather than the buoyancy forces) which is the dominant factor that determines the spatial velocity correlation functions and hence the length scales which determine the energy dissipation or rate of energy transfer from large to small scales.

Hunt's hypothesis was recently supported by Mater and Venayagamoorthy (2014). Through rigorous analyses of DNS and laboratory data, they found that the length scale of the overturning motions in the shear-dominated regime scale with L_H, whereas, in the buoyancy-dominated region, they scale with L_b. In addition, by utilizing observations from two well-known boundary layer field campaigns (CASES-99 and Surface Heat Budget of the Arctic Ocean—SHEBA), Wilson and Venayagamoorthy (2015) also found that L_H is more correlated with the classical mixing length in comparison with the buoyancy length scale. They proposed shear-based eddy-viscosity and eddy-diffusivity parameterizations and showed promising results in an idealized simulation.

In our future modelling studies (including large-eddy simulations), we intend to combine both the shear-based and buoyancy-based length scale parameterizations in a physically meaningful way. Simple interpolation approaches already exist in the literature (e.g., Grisogono and Belušić 2008; Rodier et al. 2017). An alternative approach would be to utilize a length scale proposed by Cheng and Canuto (1994) as it seems to capture the traits of both the shear-based and buoyancy-based length scales. We are currently exploring these possibilities and others.

Appendix 1: Derivation of Length Scales

Integral Length Scale: Based on the original ideas of Taylor (1935), both Tennekes and Lumley (1972) and Pope (2000) provided a heuristic derivation of the integral length scale. Given TKE ($\overline{e}$) and mean energy dissipation rate ($\overline{\varepsilon}$), an associated integral time scale can be approximated as $\overline{e}/\overline{\varepsilon}$. One can further assume $\sqrt{e}$ to be the corresponding velocity scale. Thus, an integral length scale ($\mathcal{L}$) can be approximated as $\overline{e}^{3/2}/\overline{\varepsilon}$.

In the literature, the autocorrelation function of the longitudinal velocity series is commonly used to derive an estimate of the integral length scale (L_{11}). The relationship between $\mathcal{L}$ and L_{11} is discussed by Pope (2000).

Kolmogorov Length Scale: Pope (2000) paraphrased the first similarity hypothesis of Kolmogorov (1941) as (the mathematical notations were changed by us for consistency):

"In every turbulent flow at sufficiently high Reynolds number, the statistics of the small-scale motions ($l \ll \mathcal{L}$) have a universal form that is uniquely determined by ν and $\overline{\varepsilon}$."

Based on ν and $\overline{\varepsilon}$, the following length scale can be formulated using dimensional analysis: $\eta \equiv \left(\frac{\nu^3}{\overline{\varepsilon}}\right)^{1/4}$. At this scale, TKE is converted into heat by the action of molecular viscosity.

Ozmidov Length Scale: Dougherty (1961) and Ozmidov (1965) independently proposed this length scale. Here, we briefly summarize the derivation of Ozmidov (1965). Based on Kolmogorov (1941), the first-order moment of the velocity increment (Δu) in the vertical direction (z) can be written as

$$\overline{u(z + \Delta z) - u(z)} = \overline{\Delta u} = \Delta \overline{u} \approx \overline{\varepsilon}^{1/3} \Delta z^{1/3}, \tag{22}$$

where the overlines denote ensemble averaging. Using this equation, the vertical gradient of longitudinal velocity component can be approximated as

$$\frac{\partial \overline{u}}{\partial z} \approx \frac{\Delta \overline{u}}{\Delta z} \approx \overline{\varepsilon}^{1/3} \Delta z^{-2/3}. \tag{23}$$

Similar equation can be written for the vertical gradient of the lateral velocity component ($\frac{\partial \overline{v}}{\partial z}$). Thus, the magnitude of wind shear (S) can be written as

$$S \approx \overline{\varepsilon}^{1/3} \Delta z^{-2/3}. \tag{24}$$

By definition, $Ri_g = N^2/S^2$. Thus,

$$Ri_g \approx \frac{N^2}{\overline{\varepsilon}^{2/3} \Delta z^{-4/3}}. \tag{25}$$

Ozmidov ([1965]) assumed that for a certain critical Ri_g (which is assumed to be an unknown constant), Δz becomes the representative outer length scale (L_{OZ}). Thus, Eq. 25 can be rewritten as

$$L_{OZ} \equiv \left(\frac{\overline{\varepsilon}}{N^3} \right)^{1/2}. \tag{26}$$

The unknown proportionality constant is a function of the critical Ri_g and is assumed to be on the order of one.

Corrsin Length Scale: The derivation of Corrsin ([1958]) leverages on a characteristic spectral time scale, $T_s(\kappa)$, where κ is the wavenumber, which is representative of the inertial range. Based on dimensional argument, Onsager ([1949]) proposed

$$T_s(\kappa) \equiv \frac{1}{\sqrt{\kappa^2 E(\kappa)}}. \tag{27}$$

In order to guarantee local isotropy in the inertial range, Corrsin ([1958]) hypothesized that $T_s(\kappa)$ must be much smaller than the time scale associated with mean shear (S). In other words,

$$\frac{1}{\sqrt{\kappa^2 E(\kappa)}} \ll \frac{1}{S}. \tag{28}$$

Using the $-5/3$ law of Kolmogorov ([1941]) and Obukhov ([1941a], [b]), this equation can be rewritten as

$$\frac{1}{\sqrt{\kappa^{4/3} \overline{\varepsilon}^{2/3}}} \ll \frac{1}{S}. \tag{29}$$

If we assume that for a specific wavenumber $\kappa = 1/L_C$, the equality holds in Eq. 29, then we obtain

$$L_C^{2/3} = \frac{\overline{\varepsilon}^{1/3}}{S}. \tag{30}$$

From this equation, we can estimate L_C as defined earlier in Eq. 13b.

Buoyancy Length Scale: The following heuristic derivation is based on Brost and Wyngaard ([1978]) and Wyngaard ([2010]). In an order-of-magnitude analysis, the inertia term of the Navier–Stokes equations, can be written as

$$\frac{\partial u_i}{\partial t} \sim \frac{U_s}{T_s} \sim \frac{U_s}{L_s/U_s} \sim \frac{U_s^2}{L_s}, \tag{31}$$

where L_s, T_s, and U_s represent certain length, time, and velocity scales, respectively. In a similar manner, the buoyancy term can be approximated as

$$\left(\frac{g}{\Theta_0} \right) (\theta') \sim \left(\frac{g}{\Theta_0} \right) \left(\frac{\partial \overline{\theta}}{\partial z} \right) (L_s) \sim N^2 L_s, \tag{32}$$

where Θ_0 and θ' denote a reference temperature and temperature fluctuations, respectively. Equating the inertia and the buoyancy terms, we obtain

$$L_s^2 = \frac{U_s^2}{N^2}.$$

(33)

For stably stratified flows, either $\bar{e}^{1/2}$ or σ_w can be used as an appropriate velocity scale. Accordingly, the length scale (L_s) can be approximated as $\frac{\bar{e}^{1/2}}{N}$ or $\frac{\sigma_w}{N}$. In the literature, this length scale is commonly known as the buoyancy length scale (L_b).

Hunt Length Scale Hunt et al. (1988) hypothesized that in stratified shear flows, $\bar{\varepsilon}$ is controlled by mean shear (S) and σ_w. From dimensional analysis, it follows that

$$\bar{\varepsilon} \equiv \sigma_w^2 S.$$

(34)

The associated length scale, L_H, is assumed to be on the order of σ_w/S.

Appendix 2: Energy Dissipation Rate Formulation by Weinstock (1981)

The starting point of Weinstock's derivation was the $-5/3$ law of Kolmogorov (1941) and Obukhov (1941a, b). He integrated this equation in the wavenumber space and set the upper integration limit to infinity. The lower integration limit was fixed at the buoyancy wavenumber (κ_b). Furthermore, he assumed that the eddies are isotropic for wavenumbers larger than κ_b (i.e., in the inertial and viscous ranges). His derivation can be summarized as

$$
\begin{aligned}
\frac{3}{2}\sigma_w^2 &= \int_{\kappa_b}^{\kappa_2} \alpha\bar{\varepsilon}^{2/3}\kappa^{-5/3}d\kappa \\
&= \alpha\bar{\varepsilon}^{2/3} \int_{\kappa_b}^{\kappa_2} \kappa^{-5/3}d\kappa \\
&= \frac{3\alpha}{2}\bar{\varepsilon}^{2/3} \left(\kappa_b^{-2/3} - \kappa_2^{-2/3}\right) \\
&\approx \frac{3\alpha}{2}\bar{\varepsilon}^{2/3}\kappa_b^{-2/3}.
\end{aligned}
$$

(35)

Weinstock (1981) assumed that κ_b can be parametrized by $\frac{N}{\sigma_w}$ (basically, the inverse of the buoyancy length scale L_b). By plugging this parametrization into Eq. 35 and simplifying, we obtain

$$
\begin{aligned}
\bar{\varepsilon} &\approx \sigma_w^3\kappa_b \\
&\approx \sigma_w^2 N.
\end{aligned}
$$

(36)

Appendix 3: Normalization of Variables in Direct Numerical Simulations

In DNS, the relevant variables are normalized as follows

$$z_n = \frac{z}{h}, \tag{37a}$$

$$u_n = \frac{u}{U_b}, \tag{37b}$$

$$v_n = \frac{v}{U_b}, \tag{37c}$$

$$w_n = \frac{w}{U_b}, \tag{37d}$$

$$\theta_n = \frac{\theta - \Theta_{top}}{\Theta_{top} - \Theta_{bot}}. \tag{37e}$$

After differentiation, we obtain

$$\frac{\partial u}{\partial z} = \frac{\partial u}{\partial z_n} \frac{\partial z_n}{\partial z} = \frac{\partial u}{\partial u_n} \frac{\partial u_n}{\partial z_n} \frac{\partial z_n}{\partial z} = \frac{U_b}{h} \frac{\partial u_n}{\partial z_n}, \tag{38a}$$

$$\frac{\partial v}{\partial z} = \frac{\partial v}{\partial z_n} \frac{\partial z_n}{\partial z} = \frac{\partial v}{\partial v_n} \frac{\partial v_n}{\partial z_n} \frac{\partial z_n}{\partial z} = \frac{U_b}{h} \frac{\partial v_n}{\partial z_n}, \tag{38b}$$

$$S = \sqrt{\left(\frac{\partial \overline{u}}{\partial z}\right)^2 + \left(\frac{\partial \overline{v}}{\partial z}\right)^2} = \frac{U_b}{h} S_n, \tag{38c}$$

$$\frac{\partial \theta}{\partial z} = \frac{\partial \theta}{\partial z_n} \frac{\partial z_n}{\partial z} = \frac{\partial \theta}{\partial \theta_n} \frac{\partial \theta_n}{\partial z_n} \frac{\partial z_n}{\partial z} = \left(\frac{\Theta_{top} - \Theta_{bot}}{h}\right) \frac{\partial \theta_n}{\partial z_n}. \tag{38d}$$

The gradient Richardson number can be expanded as

$$Ri_g = \frac{N^2}{S^2} = \frac{\left(\frac{g}{\Theta_0}\right)\left(\frac{\partial \overline{\theta}}{\partial z}\right)}{S^2} = \left(\frac{g}{\Theta_{top}}\right)\left(\frac{\Theta_{top} - \Theta_{bot}}{h}\right)\left(\frac{h}{U_b}\right)^2 \frac{\left(\frac{\partial \overline{\theta}_n}{\partial z_n}\right)}{S_n^2}. \tag{39}$$

Using the definition of Ri_b (see Sect. 2), we rewrite Ri_g as follows

$$Ri_g = Ri_b \frac{\left(\frac{\partial \overline{\theta}_n}{\partial z_n}\right)}{S_n^2}. \tag{40}$$

Similarly, N^2 can be written as

$$N^2 = Ri_b \left(\frac{U_b^2}{h^2}\right)\left(\frac{\partial \overline{\theta}_n}{\partial z_n}\right). \tag{41}$$

The velocity variances and TKE can be normalized as

$$\sigma_{u_n}^2 = \frac{\sigma_u^2}{U_b^2}, \tag{42a}$$

$$\sigma_{v_n}^2 = \frac{\sigma_v^2}{U_b^2}, \tag{42b}$$

$$\sigma_{w_n}^2 = \frac{\sigma_w^2}{U_b^2}, \tag{42c}$$

$$\bar{e}_n = \frac{\bar{e}}{U_b^2}. \tag{42d}$$

Following the above normalization approach, we can also derive the following relationship for the energy dissipation rate

$$\bar{\varepsilon} = \nu \left(\frac{U_b}{h}\right)^2 \bar{\varepsilon}_n. \tag{43}$$

In order to expand $\bar{\varepsilon} = \bar{e}N$, we use Eqs. 41, 42d, and 43 as follows

$$\nu \left(\frac{U_b}{h}\right)^2 \bar{\varepsilon}_n = U_b^2 \bar{e}_n Ri_b^{1/2} \left(\frac{U_b}{h}\right) \left(\frac{\partial \bar{\theta}_n}{\partial z_n}\right)^{1/2}. \tag{44}$$

This equation can be simplified to

$$\bar{\varepsilon}_n = Re_b Ri_b^{1/2} \bar{e}_n \left(\frac{\partial \bar{\theta}_n}{\partial z_n}\right)^{1/2}. \tag{45}$$

In a similar manner, $\bar{\varepsilon} = \bar{e}S$ can be re-written as

$$\bar{\varepsilon}_n = Re_b \bar{e}_n S_n. \tag{46}$$

Appendix 4: Supplementary Analyses of Simulated Data

In Fig. 5, vertical profiles of several key variables are plotted. All the profiles correspond to $T_n = 100$. Clearly, the variances and fluxes decrease with increasing cooling rate. It is also evident that stability monotonically increases with height. As a result, turbulence in the upper part of the domain becomes quasi-laminar (especially for the runs with higher cooling rates). For this reason, we did not consider data from $z/h > 0.5$ region for the computations of various length scales.

For continuously turbulent SBLs, it has been frequently observed that Ri_g stays below 0.2 within the SBL (e.g., Garratt 1982; Nieuwstadt 1984; Basu and Porté-Agel 2006). Above the SBL, in the free atmosphere, Ri_g becomes much larger. Similar behaviour is noticeable in Fig. 5 (top-right panel).

The vertical profiles of dissipation rates are shown in the bottom-right panel of Fig. 5. As expected, the dissipation rates decrease with increasing height. For $z/h < 0.1$, due to the viscous effects, the values of the dissipation rates are very high. Thus, for analyses of the length scales, we disregarded data from this region.
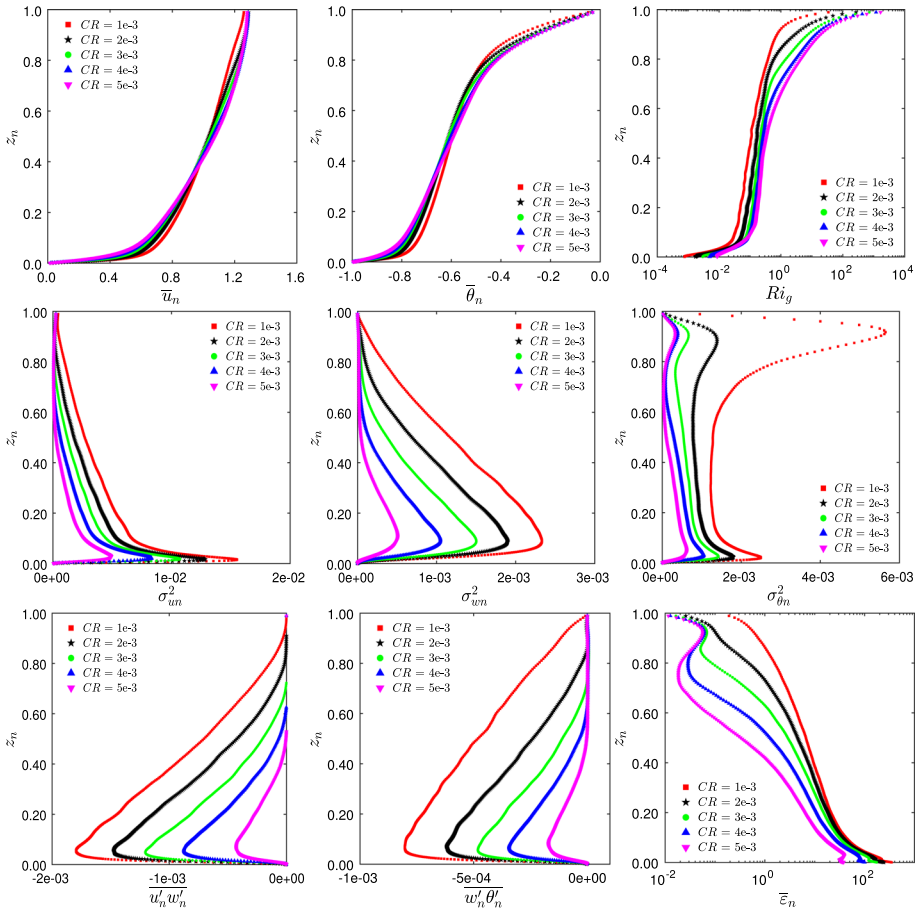
Fig. 5 Vertical profiles of normalized longitudinal velocity (top-left panel), potential temperature (top-center panel), gradient Richardson number (top-right panel), longitudinal velocity variance (middle-left panel), vertical velocity variance (middle-center panel), potential temperature variance (middle-right panel), u-component of momentum flux (bottom-left panel), sensible heat flux (bottom-center panel), and energy dissipation rate (bottom-right panel). Simulated data from five different DNS runs are represented by different coloured symbols in these plots. In the legends, *CR* represents normalized cooling rates. All the profiles correspond to $T_n = 100$

Appendix 5: Data and Code Availability

The DNS code (HERCULES) is available from: https://github.com/friedenhe/HERCULES. All the analysis codes and processed data are publicly available at http://doi.org/10.5281/zenodo.3923649. Given the sheer size of the raw DNS dataset, it is not uploaded onto any repository; however, it is available upon request from the authors.

References

Ansorge C, Mellado JP (2014) Global intermittency and collapsing turbulence in the stratified planetary boundary layer. Boundary-Layer Meteorol 153:89–116

Basu S, Porté-Agel F (2006) Large-eddy simulation of stably stratified atmospheric boundary layer turbulence: a scale-dependent dynamic modeling approach. J Atmos Sci 63:2074–2091

Bocquet F, Balsley B, Tjernström M, Svensson G (2011) Comparing estimates of turbulence based on near-surface measurements in the nocturnal stable boundary layer. Boundary-Layer Meteorol 138:43–60

Brethouwer G, Duguet Y, Schlatter P (2012) Turbulent-laminar coexistence in wall flows with Coriolis, buoyancy or Lorentz forces. J Fluid Mech 704:137–172

Brost RA, Wyngaard JC (1978) A model study of the stably stratified planetary boundary layer. J Atmos Sci 35:1427–1440

Chen WY (1974) Energy dissipation rates of free atmospheric turbulence. J Atmos Sci 31:2222–2225

Cheng Y, Canuto VM (1994) Stably stratified shear turbulence: a new model for the energy dissipation length scale. J Atmos Sci 51:2384–2396

Chung D, Matheou G (2012) Direct numerical simulation of stationary homogeneous stratified sheared turbulence. J Fluid Mech 696:434–467

Corrsin S (1958) Local isotropy in turbulent shear flow. National Advisory Committee for Aeronautics. Technical report NACA RM 58B11

Deardorff JW (1980) Stratocumulus-capped mixed layers derived from a three-dimensional model. Boundary-Layer Meteorol 18:495–527

Dougherty JP (1961) The anisotropy of turbulence at the meteor level. J Atmos Terr Phys 21:210–213

Efron B (1982) The jackknife, the bootstrap, and other resampling plans, vol 38. SIAM, Philadelphia

Flores O, Riley JJ (2011) Analysis of turbulence collapse in the stably stratified surface layer using direct numerical simulation. Boundary-Layer Meteorol 139:241–259

Foreman RJ, Emeis S (2012) A method for increasing the turbulent kinetic energy in the Mellor–Yamada–Janjić boundary-layer parametrization. Boundary-Layer Meteorol 145:329–349

García-Villalba M, del Álamo JC (2011) Turbulence modification by stable stratification in channel flow. Phys Fluids 23(045):104

Garratt JR (1982) Observations in the nocturnal boundary layer. Boundary-Layer Meteorol 22:21–48

Grisogono B (2010) Generalizing 'z-less' mixing length for stable boundary layers. Q J Roy Meteorol Soc 136:213–221

Grisogono B, Belušić D (2008) Improving mixing length-scale for stable boundary layers. Q J R Meteorol Soc 134:2185–2192

Hartogensis OK, de Bruin HAR (2005) Monin–Obukhov similarity functions of the structure parameter of temperature and turbulent kinetic energy dissipation rate in the stable boundary layer. Boundary-Layer Meteorol 116:253–276

He P (2016) A high order finite difference solver for massively parallel simulations of stably stratified turbulent channel flows. Comput Fluids 127:161–173

He P, Basu S (2015) Direct numerical simulation of intermittent turbulence under stably stratified conditions. Nonlinear Proc Geophys 22:447–471

He P, Basu S (2016a) Development of similarity relationships for energy dissipation rate and temperature structure parameter in stably stratified flows: a direct numerical simulation approach. Environ Fluid Mech 16:373–399

He P, Basu S (2016b) Extending a surface-layer c_n^2 model for strongly stratified conditions utilizing a numerically generated turbulence dataset. Opt Express 24:9574–9582

Hunt JCR, Stretch DD, Britter RE (1988) Length scales in stably stratified turbulent flows and their use in turbulence models. In: Puttock JS (ed) Stably stratified flow and dense gas dispersion. Clarendon Press, Oxford, pp 285–321

Hunt J, Moin P, Lee M, Moser RD, Spalart P, Mansour NN, Kaimal JC, Gaynor E (1989) Cross correlation and length scales in turbulent flows near surfaces. In: Fernholz HH, Fiedler HE (eds) Advances in turbulence 2. Springer, New York, pp 128–134

Itsweire EC, Koseff JR, Briggs DA, Ferziger JH (1993) Turbulence in stratified shear flows: implications for interpreting shear-induced mixing in the ocean. J Phys Ocean 23:1508–1522

Janjić ZI (2002) Nonsingular implementation of the Mellor–Yamada level 2.5 scheme in the ncep meso model. National Centers for Environmental Prediction, Office Note No. 437. Technical report

Kolmogorov AN (1941) The local structure of turbulence in incompressible viscous fluid for very large Reynolds numbers. Dokl Akad Nauk SSSR 30:299–303 **(english translation)**

Mater BD, Venayagamoorthy SK (2014) A unifying framework for parameterizing stably stratified shear-flow turbulence. Phys Fluids 26:036601

Mater BD, Schaad SM, Venayagamoorthy SK (2013) Relevance of the Thorpe length scale in stably stratified turbulence. Phys Fluids 25(076):604

Mellor GL, Yamada T (1982) Development of a turbulence closure model for geophysical fluid problems. Rev Geophys Space Phys 20:851–875

Mooney CF, Duval RD (1993) Bootstrapping: a nonparametric approach to statistical inference, vol 95. Sage, Thousand Oaks, p 73

Nakanishi M (2001) Improvement of the Mellor–Yamada turbulence closure model based on large-eddy simulation data. Boundary-Layer Meteorol 99:349–378

Nieuwstadt FTM (1984) The turbulent structure of the stable, nocturnal boundary layer. J Atmos Sci 41:2202–2216

Obukhov AM (1941a) On the distribution of energy in the spectrum of turbulent flow. Dokl Acad Nauk SSSR 32:22–24

Obukhov AM (1941b) Spectral energy distribution in a turbulent flow. Izv Akad Nauk SSSR Ser Geogr Geofiz 5:453–466

Onsager L (1949) Statistical hydrodynamics. Nuovo Cimento Ser 9(6):279–287

Ozmidov RV (1965) On the turbulent exchange in a stably stratified ocean. Izv Acad Sci USSR Atmos Oceanic Phys 1:853–860

Pope SB (2000) Turbulent flows. Cambridge University Press, Cambridge, p 771

Rodier Q, Masson V, Couvreux F, Paci A (2017) Evaluation of a buoyancy and shear based mixing length for a turbulence scheme. Front Earth Sci 5:65

Schumann U, Gerz T (1995) Turbulent mixing in stably stratified shear flows. J Appl Meteorol 34:33–48

Shah SK, Bou-Zeid E (2014) Direct numerical simulations of turbulent Ekman layers with increasing static stability: modifications to the bulk structure and second-order statistics. J Fluid Mech 760:494–539

Smyth WD, Moum JN (2000) Length scales of turbulence in stably stratified mixing layers. Phys Fluids 12:1327–1342

Sorbjan Z, Balsley BB (2008) Microstructure of turbulence in the stably stratified boundary layer. Boundary-Layer Meteorol 129:191–210

Taylor GI (1935) Statistical theory of turbulence. Proc R Soc Ser A 151:421–444

Tennekes H, Lumley JL (1972) A first course in turbulence. MIT Press, Cambridge, p 300

Thiermann V, Grassl H (1992) The measurement of turbulent surface-layer fluxes by use of bichromatic scintillation. Boundary-Layer Meteorol 58:367–389

Vassilicos JC (2015) Dissipation in turbulent flows. Ann Rev Fluid Mech 47:95–114

Weinstock J (1981) Energy dissipation rates of turbulence in the stable free atmosphere. J Atmos Sci 38:880–883

Wilson JM, Venayagamoorthy SK (2015) A shear-based parameterization of turbulent mixing in the stable atmospheric boundary layer. J Atmos Sci 72:1713–1726

Wyngaard JC (1973) On surface-layer turbulence. In: Haugen DA (ed) Workshop on micrometeorology. AMS, New York, pp 101–149

Wyngaard JC (2010) Turbulence in the atmosphere. Cambridge University Press, Cambridge, p 393

Wyngaard JC, Coté OR (1971) The budgets of turbulent kinetic energy and temperature variance in the atmospheric surface layer. J Atmos Sci 28:190–201

Wyngaard JC, Izumi Y, Collins SA (1971) Behavior of the refractive-index-structure parameter near the ground. J Opt Soc Am 61:1646–1650